



HAL
open science

Searching for ancient pits and voids at the Ouels Mine (Castel-Minier, France) by using geophysical methods

Florsch Nicolas, Lucia Seoane, Muriel Llubes, Florian Téreygeol

► To cite this version:

Florsch Nicolas, Lucia Seoane, Muriel Llubes, Florian Téreygeol. Searching for ancient pits and voids at the Ouels Mine (Castel-Minier, France) by using geophysical methods. *Journal of Archaeological Science: Reports*, 2024, 57, pp.104624. 10.1016/j.jasrep.2024.104624 . hal-04786790

HAL Id: hal-04786790

<https://hal.science/hal-04786790v1>

Submitted on 16 Nov 2024

HAL is a multi-disciplinary open access archive for the deposit and dissemination of scientific research documents, whether they are published or not. The documents may come from teaching and research institutions in France or abroad, or from public or private research centers.

L'archive ouverte pluridisciplinaire **HAL**, est destinée au dépôt et à la diffusion de documents scientifiques de niveau recherche, publiés ou non, émanant des établissements d'enseignement et de recherche français ou étrangers, des laboratoires publics ou privés.

1 **Title: Searching for ancient pits and voids at the Ouels Mine (Castel-Minier,**
2 **France) by using geophysical methods**

3
4 Authors:

5
6 Florsch Nicolas⁽¹⁾ , Seoane Lucia⁽²⁾, Llubes Muriel⁽²⁾, Téreygeol Florian⁽³⁾

7
8 (1) Sorbonne Université, UMI 209 UMMISCO, 4 place Jussieu, 75005 Paris,
9 France

10 (2) Université Paul Sabatier, OMP-GET, UMR 5563, CNRS/IRD/UPS, 14 Avenue
11 Edouard Belin, 31400 Toulouse, France

12 (3) LAPA, UMR 7065 IRAMAT and UMR 3685 NIMBE, CEA, CNRS, Université
13 Paris-Saclay, CEA Saclay, 91191 Gif-sur-Yvette, France

14
15
16 **Abstract**
17

18 A map from the early twentieth century shows the relative positions of several
19 entrances to the Ouels mining area, but it is not fully georeferenced. Some mines
20 have been reported in the south-western part of the map and the archaeological
21 team would like to confirm these locations. To this end, a geophysical prospection
22 campaign was organised, which included electrical resistivity tomography (ERT) and
23 microgravimetric profiling over the area of interest. Several anomalies were identified.
24 Two of them, in the north, are very likely to be related to voids (robbed area), since
25 gravimetric and electrical anomalies are superimposed. Conversely, in the southern
26 part, where microgravimetric anomalies occur, there are no electrical anomalies, but
27 cavities could be electrically shielded by the overburden. An additional deeper ERT
28 shows a new but small resistivity anomaly in the upper slope, outside the area
29 preliminarily surveyed. Although not all of the gravimetric anomalies are confirmed by
30 the ERT, the geophysics ultimately proved very effective in supporting at least some
31 archaeological targets in the northern part of the prospect.

32
33 **1. Introduction**

34
35 *1.1. Archaeological context*

36
37 Mining archaeology " a continuously increasing but still emerging branch of
38 archaeology." It suffers mainly from the difficulty of accessing the underground.
39 Entrances to galleries and shafts are often blocked. It takes a lot of time and effort for
40 the researcher to get to the areas of interest, with the risk of ending up in collapsed
41 and scientifically unusable areas. The development of prospective methods that allow
42 the volume of existing cavities to be assessed before the first shovel is used, as well
43 as the extension of the discovery to be treated, therefore appears to be a major
44 challenge for this discipline. It is a question of making it possible to study the mining
45 systems that provide the raw material for all metallurgy, whatever the period under

46 consideration. The example we are developing here is no exception to the rule, but is
47 firmly in line with a methodological framework for future archaeological interventions.
48

49 The Ouels mining network in Castel-Minier was the subject of several more or less
50 intensive mining operations between the 10th and 20th centuries. It is located near
51 Aulus-les-Bains in the department of Ariège, France (see Fig. 1). The most important
52 works seem to have been carried out between the end of the 13th century and the
53 turn of the 16th century (Téreygeol, 2023). In the Middle Ages, the mine was owned
54 by the Viscount of Couserans. This viscounty was part of the county of Comminges,
55 an autonomous state with links to both the Crown of Aragon and the Crown of
56 France. (Higounet; 1947). At the beginning of the 14th century, the mine seems to
57 have been one of the most important in the Pyrenees, delivering one tonne of silver a
58 year (Bailly-Maitre, Benoit, 1998). Thanks to the most recent exploitation, which
59 ended after the First World War, we have access not only to modern exploitation
60 areas, but also to much older ones. However, a large part of the network has been
61 gradually filled in. Several mining sectors, although known from old documents,
62 remain inaccessible to us.

63 Since 2003, several geophysical surveys have been carried out on the right bank of
64 the Garbet (e.g. Bonnamour et al. 2007, Florsch et al. 2011 and Florsch et al. 2012).
65 If the deposit and the mine are well located, an archaeological operation in a mine
66 must be carried out at the access points, which must be geolocated as accurately as
67 possible. Above all, we need to be able to estimate the scale of the required
68 excavation work to study these mining networks. It is therefore essential to gather as
69 much information as possible prior to the archaeological work, in particular to
70 determine whether there are any accessible voids. This work can be carried out using
71 traditional speleological techniques, but in mining areas where access is unknown,
72 geophysics must be used prior to any major archaeological work. This is the case
73 here, based on both surface anomalies observed at the site and a 1913 mining plan.



74

75 **Fig. 1.** Mine district “ Les Ouels” located in the south of France.

76

77 *1.2. Geology, mineralogy and documented historical mines*

78

79

80 The mining network is located in the central part of the northern slope of the
 81 Pyrenees, where the highest peaks of this massif are concentrated. This area is
 82 crossed by the North Pyrenean Fault, which in our case is materialised by the Garbet
 83 stream. On the right bank, the terrain is of Post-Hercynian age, whereas on the left
 84 bank it is mainly Devonian (Laforêt et. al. 1983).

85

86 The deposit that supports the mine is of hydrothermal type and was emplaced in
 87 Paleozoic sedimentary terrains. It lies between Silurian shales (-443.4 to -419.2 Ma)
 88 to the north and Devonian dolomites (-419.2 to -358.9 ±0.4 Ma) to the south. The
 89 mineralisation is of vein type. It occurs in two parallel veins at the shale-dolomite
 90 contact and directly in the dolomite. They strike N 120°E to N 140°E (Dubatik et. al.
 91 1981).

92

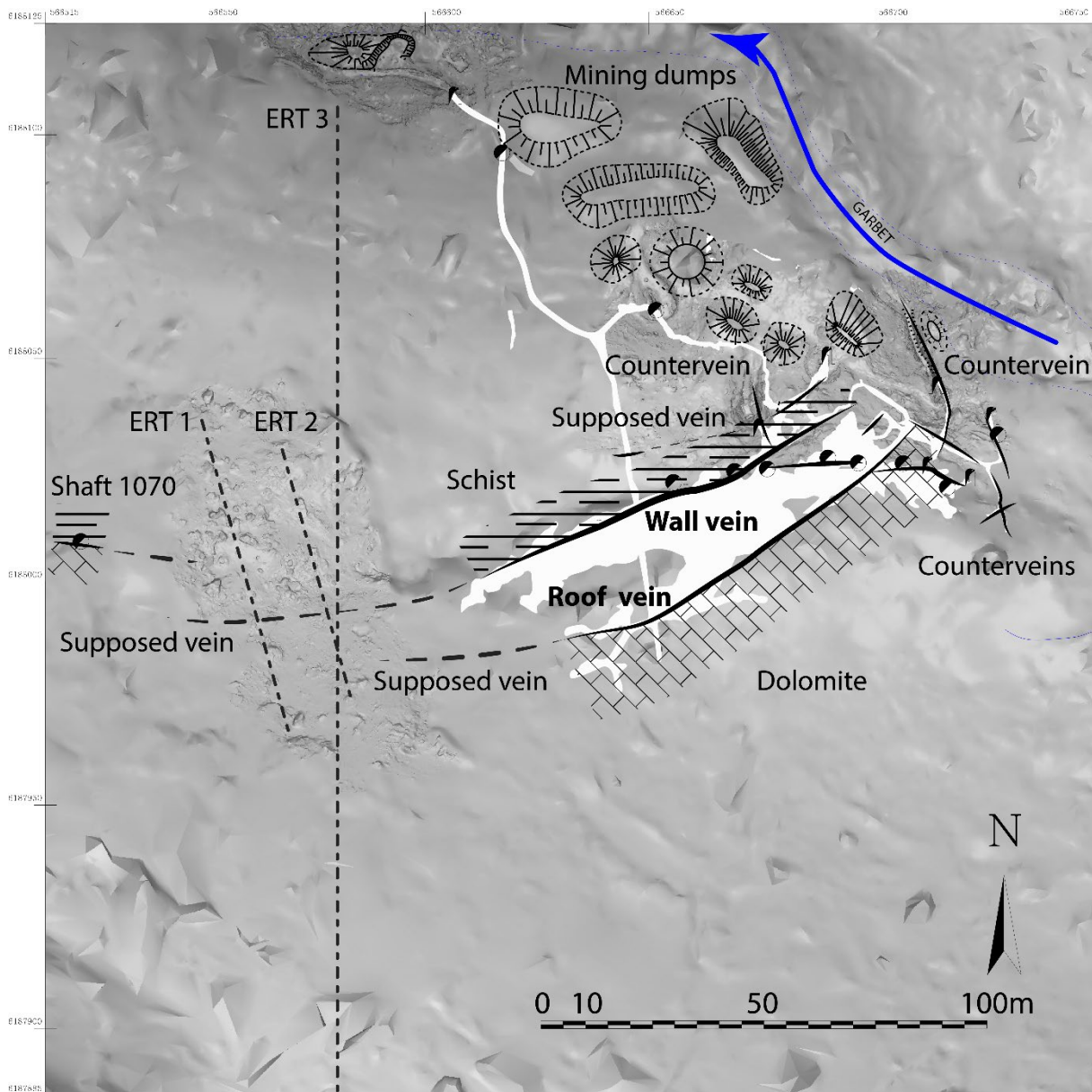
93 The mineralisation consists mainly of galena, sphalerite and chalcopyrite in a vein
 94 system that varies from calcite to quartz, depending on what is still visible in the
 95 workings. The silver, which is at the heart of this exploitation, is present in the galena,
 96 sometimes in the sphalerite. It also accompanies the grey copper. This last
 97 mineralisation, as well as the bournonite, is only known through the ores found during
 98 the archaeological excavations of the surface workshops located on the other bank of
 99 the Garbet (Flament et. al. 2019). Thus, this research is of interest to both

100 archaeology and mineralogy, and contributes to the advancement of knowledge in
101 these two fields.

102

103 The above-mentioned vein zone is developed at the contact between dolomites and
104 shales, as shown in Fig. 2. There is no other detailed geological mapping of the area
105 around this zone (existing geological maps are only at 1: 50,000 scale and show no
106 detail).

107



108

109 Fig. 2. Mineralized vein and its surroundings, with dolomites to the south and shales
110 to the north. We have also traced the resistivity sections ERT1 to ERT3 (dotted
111 lines).

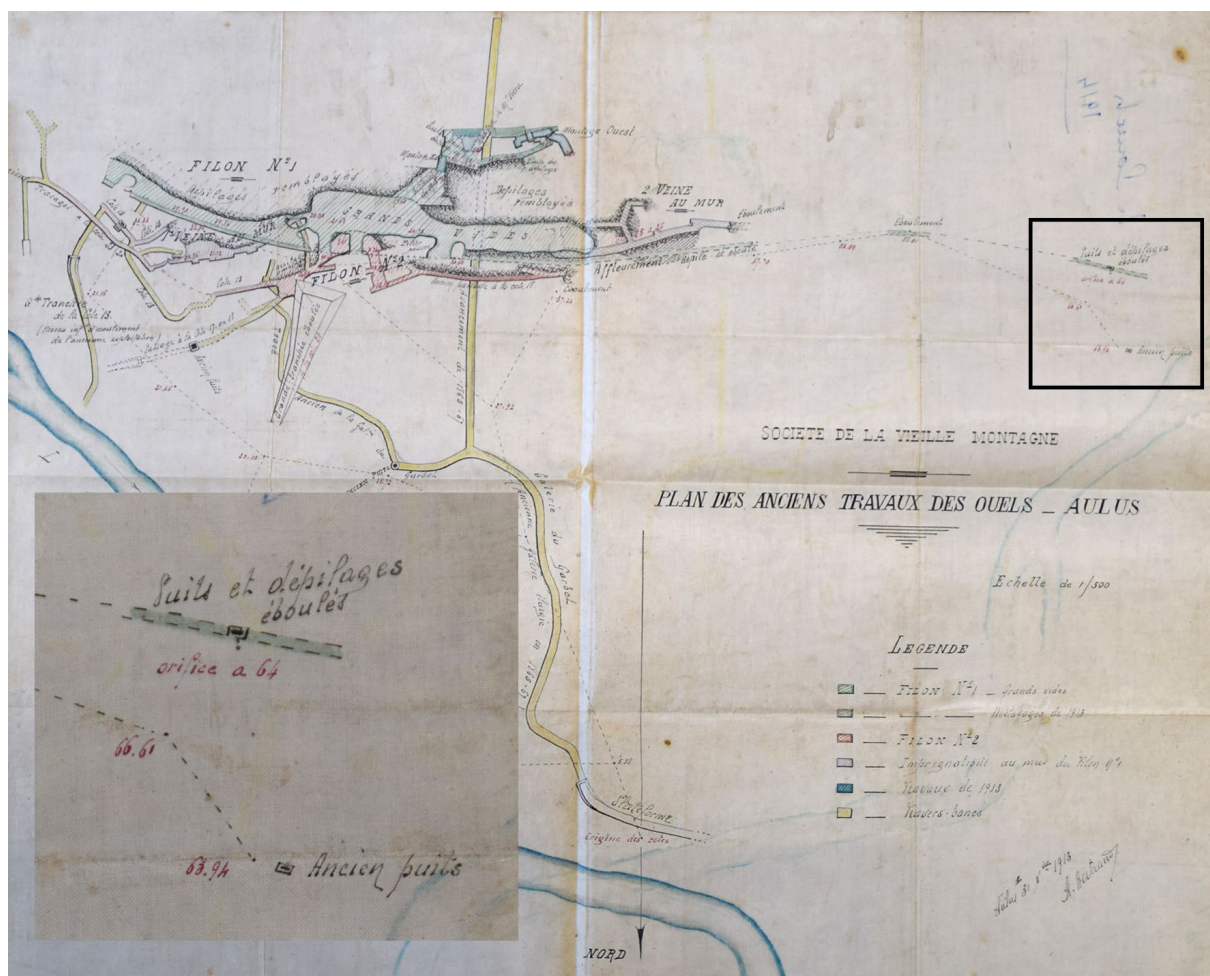
112

113

114 One of these veins, the hanging wall vein, is easily accessible through several shafts
115 and galleries. Its location is particularly easy to see on the surface. It follows a

116 dolomitic wall at the foot of which a series of drill holes are still accessible.
 117 Conversely, the footwall vein has only been explored in small sections, mainly
 118 through rare connections with the hanging wall vein network, and always in the lower
 119 eastern half of the mineralised panel. It is this vein that we are focusing on. We have
 120 an archive plan from the last mining attempt in the early 20th century. On the 1913
 121 mine plan (Fig. 3), the engineer has two pieces of information that are essential to
 122 our study: an extension of the formerly mined lode in its western extension with the
 123 mention of "shafts and crumbling deposits, orifice" at 64 shoreline, and the
 124 positioning of an "old shaft" at 68.94 shoreline, which is within a radius of 145 m of
 125 the "large trench". This shaft is also 14 m north of the hanging wall vein.
 126 Underground, our reconnaissance indicates that the veins are blocked at a distance
 127 of 50 m from the location of the supposed shaft. In particular, this blockage is
 128 observed at the base of the deposit at level 0, whereas the supposed shaft head is at
 129 +70 m. This difference in level makes any attempt to re-open illusory and
 130 disproportionate, unless we are sure that the overburden forms a plug at the surface
 131 and that there are empty spaces to be explored.

132
 133 In fact, the topographical locations mentioned in ancient documents are not precisely
 134 georeferenced and are therefore only a guide for the archaeologist. This is why
 135 geophysical surveys are required to pinpoint, if possible, the location of significant
 136 voids in this upper part of the claim.
 137



138
 139

140 **Fig. 3.** Mine plan from 1913. It shows the knowledge at the beginning of the 20th century as
141 represented by the engineers. The small enlarged square marks our area of interest, with
142 two pits. Note that the north faces downwards.

143

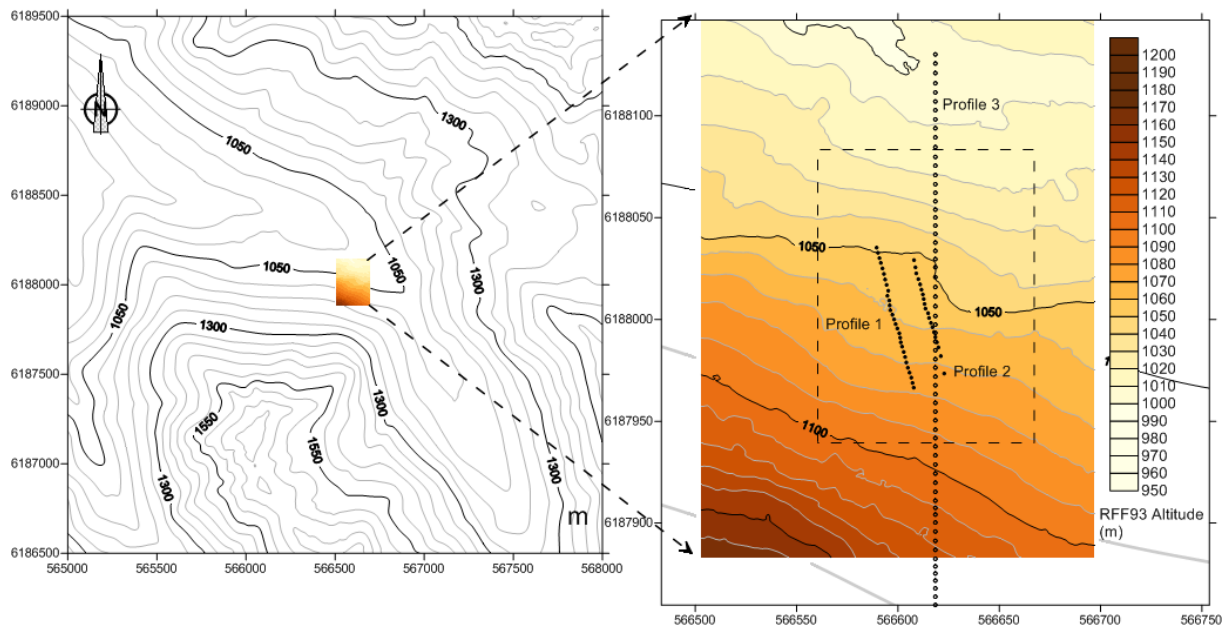
144 2. Materials and methods

145 2.1. Topography and survey induced constraints

146

147

148 Fig. 4 shows the surrounding topography with an enlarged central coloured area on
149 the right. The latter also shows the gravimetric profile location (in red) and the three
150 electrical resistivity tomographies (ERT) performed (shown in black). The dots are
151 real electrode positions. Two of the ERTs are classified as "shallow" with an
152 electrode spacing of 1.5 m, while the large one, strictly N-S, is classified as "deep"
153 with an electrode spacing of 5 m.



154

155 **Fig. 4.** DEM of the area, 3 km × 3 km with a 5 m × 5 m grid in the periphery and a coloured
156 central area of 1 m × 1 m. The large mesh is derived from data of French IGN (National
157 Geographical Institute), while the small mesh is a mixture of LIDAR overflight and ground
158 photogrammetry. Black points are relative to the ERT with two short profiles (1.5 m spacing)
159 and one large profile exactly NS (5 m spacing). Coordinates are Lambert 93 in RGF 93
160 metric system.

161

162 From the geophysicist's point of view, the conformation of the site leads to several
163 practical difficulties. Slopes often approach 100%. Some boulders are present and
164 the bedrock is regularly outcropping in many places. Tree stumps and snags lie on
165 the ground and the field is actually covered by a deciduous forest. Colluviation is
166 important, and the thickness of the colluvium is irregular: sometimes the bedrock
167 outcrops, and a few metres laterally it can be several metres deep. Fig. 5 illustrates

168 these field conditions and shows a measurement with the gravimeter in this
169 environment.

170

171 *2.2. Gravimetrical field procedure*

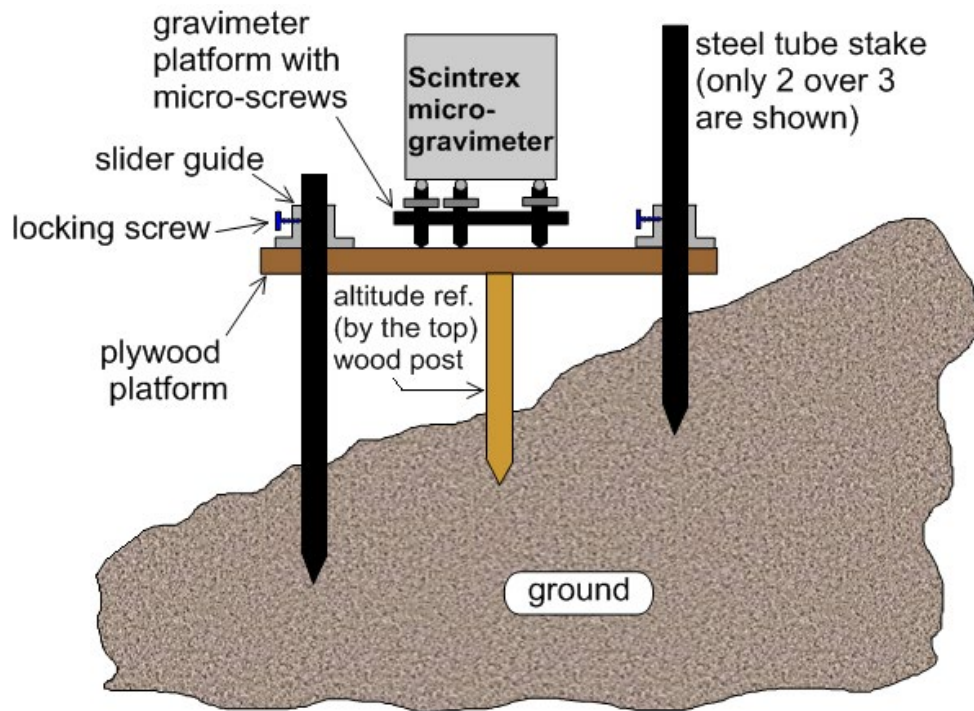


172

173 **Fig. 5.** This picture shows the ground conditions. The gravimeter is leveled using the
174 Gravimeter 3 micrometer screw system, but a special plywood platform has been designed
175 to make the instrument easier to set up. Without this, levelling would have been extremely
176 difficult, if not impossible. This platform is shown in detail in Fig. 6.

177

178 A special platform has been built to facilitate the gravimeter stationing, it is shown on
179 Fig. 5 and a drawing plus one photo on Fig. 6 shows the platform design in more
180 detail.



181

182 **Fig. 6.** Design and photo of the first platform installed. It consists of three sliding feet that
 183 move vertically thanks to three vertical guides. The sliding tubes are locked with screws once
 184 the mobile posts are in place. The wooden platform is levelled thanks to a level indicator, so
 185 that the levelling of the gravimeter requires a minimum and residual work. This system can
 186 cope with high slopes despite loose ground, while the posts can be driven 10 to 40 cm deep.

187

188

189 All these soil conditions do not facilitate measurement. Special precautions must
190 therefore be taken to ensure the quality of the measurement and post-processing, as
191 described below.

192

193 *2.3. Construction of the local DEM for gravimetry data processing and ERT.*

194

195 Creating a suitable DEM (Digital Elevation Model) is not just a matter of data location
196 or environment description. For electrical tomography, the classical 2.5D approach
197 requires at least the relative altitude of the electrodes. This allows us to take into
198 account the main topographic effects affecting electrical measurements, while true
199 3D effects are generally more or less rightly neglected when using software such as
200 RES2DINV (Loke 2000 and 2011). This means that taking into account the true
201 surface topography will obviously affect the inversion results, but less so than
202 neglecting the 3D reality of the subsurface, which is not investigated in 2.5 surveys
203 anyway. This compromise is accepted because it does not generally ruin the
204 tomography results, although it may lead to a few percent uncertainties in the
205 tomography that remain acceptable.

206 An accurate DEM is much more critical when used for microgravimetry. There are
207 two levels of topographic issues. On the one hand, the height of the measurement
208 points must be accurately determined in order to make accurate free-air corrections.
209 Since one centimetre of height corresponds to a variation of 3 μGal , and since one
210 wants to be close to μGal accuracy, the levelling of the measurement points must be
211 better than, say, ± 2 mm (this is for the "free air effect" correction). To obtain this
212 accuracy and to maintain it during the campaign, the measuring point is materialised
213 by a wooden stake of at least 30 cm length (or more) that one buries to leave about
214 10 cm above the ground. The platform supporting the gravimeter, of constant
215 thickness, is then placed on top of the stake and its horizontality is adjusted using the
216 sliding tripod and a spirit level. On top of this plywood platform, the commercially
217 available microscrew tripod associated with the gravimeter is placed. As a
218 precaution, one of the screws of this platform is blocked during the whole campaign
219 to ensure that the vertical offset of this tripod remains strictly constant over time.

220 A trade-off must be made between the requirements for altitude accuracy and the
221 time spent in the field. Assuming that the altitude of the stakes is known to be, say, 2
222 mm (in relative terms), and that the rest of the errors are of the same order or
223 magnitude, we conclude that no better than 2 μGal accuracy (RMS) could be
224 achieved in this levelling operation.

225 The second point relates to terrain corrections. Traditionally, in addition to correcting
226 for instrumental drift, tidal and latitudinal effects, one has to take into account the
227 attraction of the surrounding topography, traditionally dividing this direct Newtonian
228 effect into two contributions, the so-called "Bouguer effect" and the "terrain effect".
229 The Bouguer effect is the attraction due to an infinite plate between your height and a
230 reference height that you choose at the beginning of the survey. If your terrain is flat,
231 there is no additional effect to consider. But if it is not, you need to take into account
232 the relief, the difference between the actual topography and a horizontal surface. For
233 example, if you are at the foot of a hill, the hill will have a direct upward Newtonian
234 attraction, reducing the gravity field that would exist without it.

235 Further details on topography are given in the sections devoted to the two methods
236 used in this study. For details of the gravimetric or the electrical resistivity
237 tomography methods themselves, the reader will benefit from reading Loke 2000 and
238 2011 or the recent book by Binley and Slater, 2020. For gravimetry, one of the best
239 books that contains everything you ever wanted to know about this method is that by
240 Blakely (1995).

241 The topography we use here includes an "outer part" based on the IGN 5m datum
242 (Institut Geographique National), but in the central area we have combined lidar data
243 (1 m lateral resolution) and photogrammetry, which is more suitable for accurate
244 altitude, especially as far as gravimetry is concerned. The central area corresponds
245 to the coloured rectangle in Fig. 4. The precise heights of the reference gravimetric
246 stakes were measured (with an accuracy of about 3 mm equivalent to 1 μ Gal) using
247 a Leica total station tachometer in a local altimetric reference system, before
248 referencing these data to the French RGF93 reference system.

249

250

251 *2.4. Deployment of gravimetric and ERT methods*

252

253 The subsurface and degree of geological heterogeneity preclude the use of some of
254 the most powerful geophysical techniques such as GPR (Ground Penetrating Radar),
255 IEM (Induced ElectroMagnetism) or MASW (Multichannel Analysis of Surface
256 Waves). They would have been relevant in a less harsh topographic context, but not
257 here.

258 Since the aim is to detect robbed cavities, microgravimetry is the first suitable method
259 that comes to mind. Gravimetry is one of the rare "direct" methods in the sense that it
260 directly detects the lack (or excess) of mass (density directly affects the gravitational
261 field). Moreover, our targets (robbed caves) are scaled in such a way that gravimetry
262 is effectively applied: they are large enough to produce significant and undeniable
263 anomalies. Thanks to the ever-increasing accuracy of gravimeters, microgravimetry
264 is increasingly being used in archaeology, see for example Eppelbaum (2010), and
265 Paštka et al. (2000).

266 The second appropriate method, ERT, is chosen because robbing voids are large
267 enough to justify a significant resulting resistivity anomaly. The method is indirect:
268 only a very resistive body will give an anomaly similar to that due to a void. It's not
269 because the current doesn't cross that you have a cavity, it may just be very resistive
270 in appearance. In this case, based on previous resistivity campaigns in the area, it is
271 assumed that the surrounding resistivity extent is capped, and then a very high
272 resistivity underlines with high probability the presence of a cavity, if there is one.

273

274 The profile implementation for ERT methods has already been shown in Fig. 4. The
275 gravimetric profiles are shown on Fig. 10 (blue dots) They are oriented to be more or
276 less perpendicular to the expected robbed and to respond to the field practical
277 conformation.

278 Another archaeological example of combining microgravimetry with electrical
279 tomography can be found, for example, in Paštka et al. (2019). Other extensive
280 archaeological studies of ancient mines can be cited, such as Hruby et. Al. 2021 and

281 Trebsche et. al., 2022. Note, however, that they do not look for cavities, but mainly
282 for metallurgical targets, at least as far as geophysics is concerned.

283
284

285 The instrument, a Scintrex CG-5M (relative gravimeter), is shown in operation in Fig.
286 5. A relative precision of 1 μGal is theoretically achievable, provided a careful
287 procedure is followed. Over a small range altitude interval, the accuracy is equal to
288 the precision. However, in the context of such a campaign in the forest and under
289 rather harsh conditions, the realistic repeatability (then precision) is probably around
290 5 μGal . This can be trusted by following a procedure of taking 3 measurements (each
291 lasting 2 min) and then taking the median of these three, but a loss of accuracy also
292 results from the topographical conditions. Classical corrections, such as those for
293 time drift (which turns out to be very linear when using this instrument), air-free,
294 Bouguer (or "plateau"), tidal and latitudinal effects are easily obtained. The
295 calculation of the tidal effect itself is a built-in service of the gravimeter, requiring the
296 setting of UCT and geographical coordinates thanks to the instrument's configuration
297 facilities. The only correction that requires further discussion here is the terrain
298 correction.

299 Terrain corrections are processed to make the effect of relief negligible. In fact,
300 gravimetry is based on Newton's universal law of attraction. Therefore, any
301 surrounding mass will affect the measurement. For a given volume of the subsurface,
302 this gravitational effect depends on density. However, it is impossible to assess in
303 detail the density distribution near (or far!) from the instrument. In addition, one has to
304 rely on a mean density value that is assumed to be known or has to be determined.

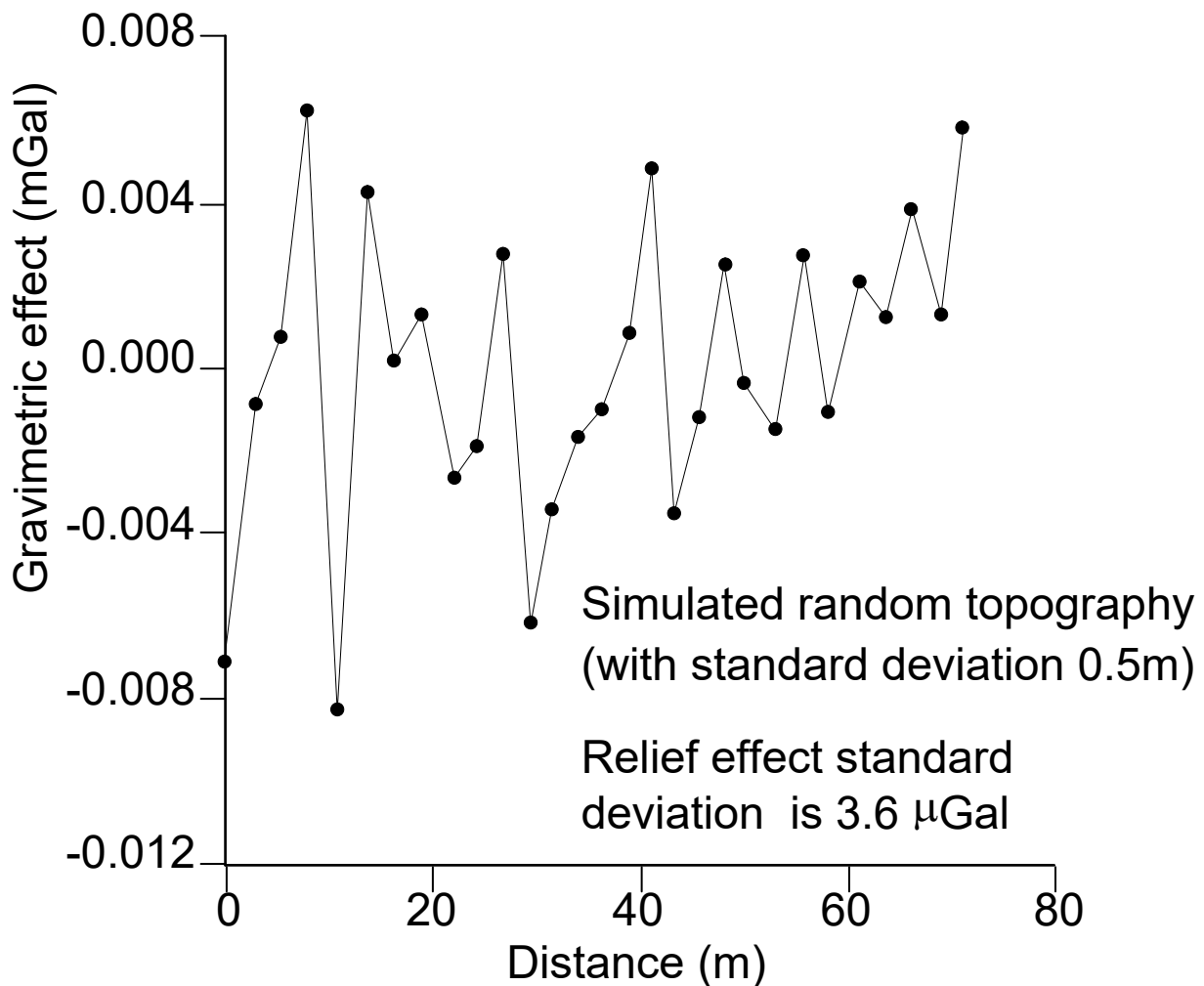
305 This average density is at least needed to calculate the terrain correction. A way to
306 determine an average density for the terrain correction is very simple: just try different
307 values, for example from 2 to 3 in 0.1 steps, and keep the density that gives a
308 minimum correlation between the relief and the fully corrected gravity map: this is the
309 density to use (this is called the Nettleton method, (1939)). Note that it is the same
310 density that must be used for the Bouguer (plateau) correction; both effects (plateau
311 and terrain) are relative to the same environment. In short, it would be ideal to know
312 the entire surrounding density in 3D, but this is not possible in practice or even in
313 theory (without digging everywhere).

314 Now a question arises: what resolution (lateral and vertical) does a DEM need to be
315 known in order to get a "good" measurement (better than 3 μGal)? There are several
316 ways to answer this question. A simple pragmatic way is to perturb the given grid
317 (e.g. 1m \times 1m) and evaluate the effect on the corresponding theoretical gravimetric
318 map. Note that a DEM grid thinner than 1 \times 1m would question the very meaning of
319 what constitutes a surface topography: would we be taking into account boulders of
320 0.5m size, tree stumps, and this question is compounded by the fact that there may
321 be boulders or stumps just below the surface that you will never know about. The
322 geophysicist (and other people) have to accept a compromise. The rule of thumb is:
323 we stop the effort in the correction process by following the idea that we invest work
324 until we reach acceptable errors within the framework of the method and the
325 objective.

326 Let us imagine a benchmark dedicated to this procedure. In Fig. 7, we show the
327 gravity variations induced by varying the altitude of the points (on a 1m \times 1m grid),

328 following a uniform probability density function (pdf) within a +/- 50 cm interval. This
 329 is a relatively blunt assumption, as it could represent the error in modelling the
 330 topographic model by interpolation within the 1m x 1m grid. We note that the
 331 resulting gravity standard deviation (SD) is less than 4 μ Gal, and we consider this
 332 satisfactory in our context: our "surface knowledge" is better than 50 cm (but
 333 remember that we are ignorant of possible subsurface heterogeneities, buried rock
 334 blocks, etc.).

335



336

337 **Fig. 7.** Simulation of the fluctuation of the gravitational field assuming the uncertainty (real or
 338 interpolated) of the topography of our field. From this result we conclude that our corrections
 339 are quite realistic within an interval of +/- 5 μ Gal.

340

341 *2.5. Gravimetric results and models*

342

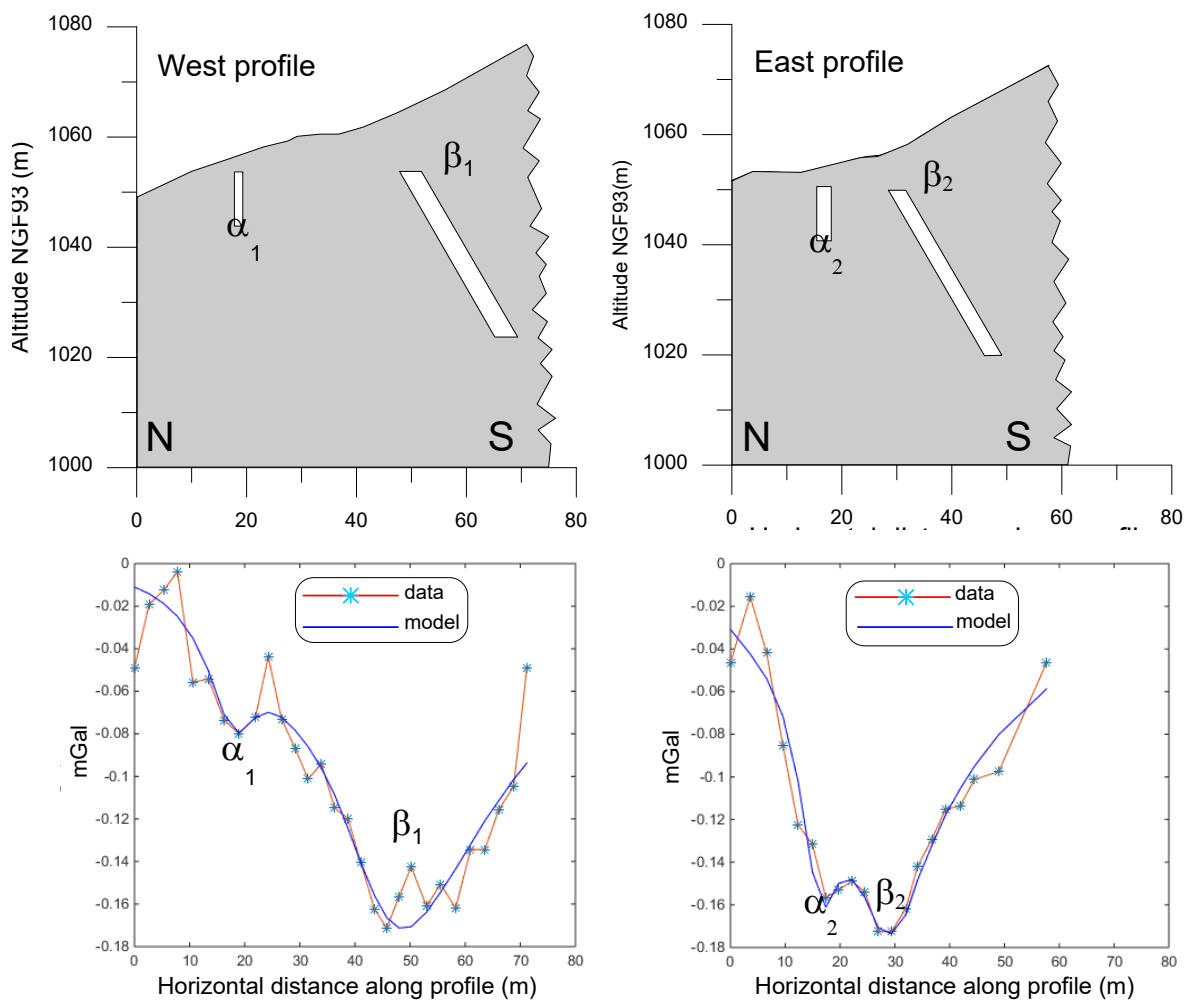
343 Fully corrected data (from drift, tide, free air, Bouguer, topography) are shown in the
 344 lower part of Fig. 8 with two superimposed curves: data (red lines) and computed
 345 modelled anomalies (blue line) derived using the models shown in the upper part of
 346 the figure. The eastern fit appears to be of better quality (or success) than the

347 western one. Discrepancies can locally reach 20 μGal , which can be considered as
348 random outliers with respect to our standard deviation of 5 μGal .

349
350 These interpretations were obtained using a blind approach, i.e. with no prior
351 assumptions other than that the structures are centred on the profile and extend for
352 200 m in the direction perpendicular to the profile. This is consistent with the likely
353 geological configuration of the mine voids on the site. A manual error and trial
354 approach was preferred to a blind inversion where a priori knowledge would have
355 been difficult to incorporate. In particular, the dip of the void was chosen to match the
356 known dip of the fault.

357
358 Of course, one could judge that these interpretations are trustworthy by noting that
359 the fit is satisfactory. In fact, this would be to forget that the gravimetric interpretation
360 model can present an extreme variability. As is often the case in geophysics, and
361 especially when dealing with potential methods, the fit can be satisfactory but the
362 relative interpretation variable (this is an aspect of the non-unicity of the solution in
363 the inverse problem, see for example Tarantola, 2005). This may come back to haunt
364 us.

365



366

367 **Fig. 8.** West and East cavity models (top), data in red line and modelled anomalies in blue
368 line (bottom). The Greek letters are relative to the positions shown in Fig. 10. These

369 anomalies are computed along the topography where the gravimetric measurements lie
370 (even after relief corrections).

371
372 *2.6. Electric tomography settlement and results*

373 Electrical methods in geophysics have been used worldwide since Conrad
374 Schlumberger published his book (1920). Modern developments include electrical
375 tomography (Binley and Slater 2020).

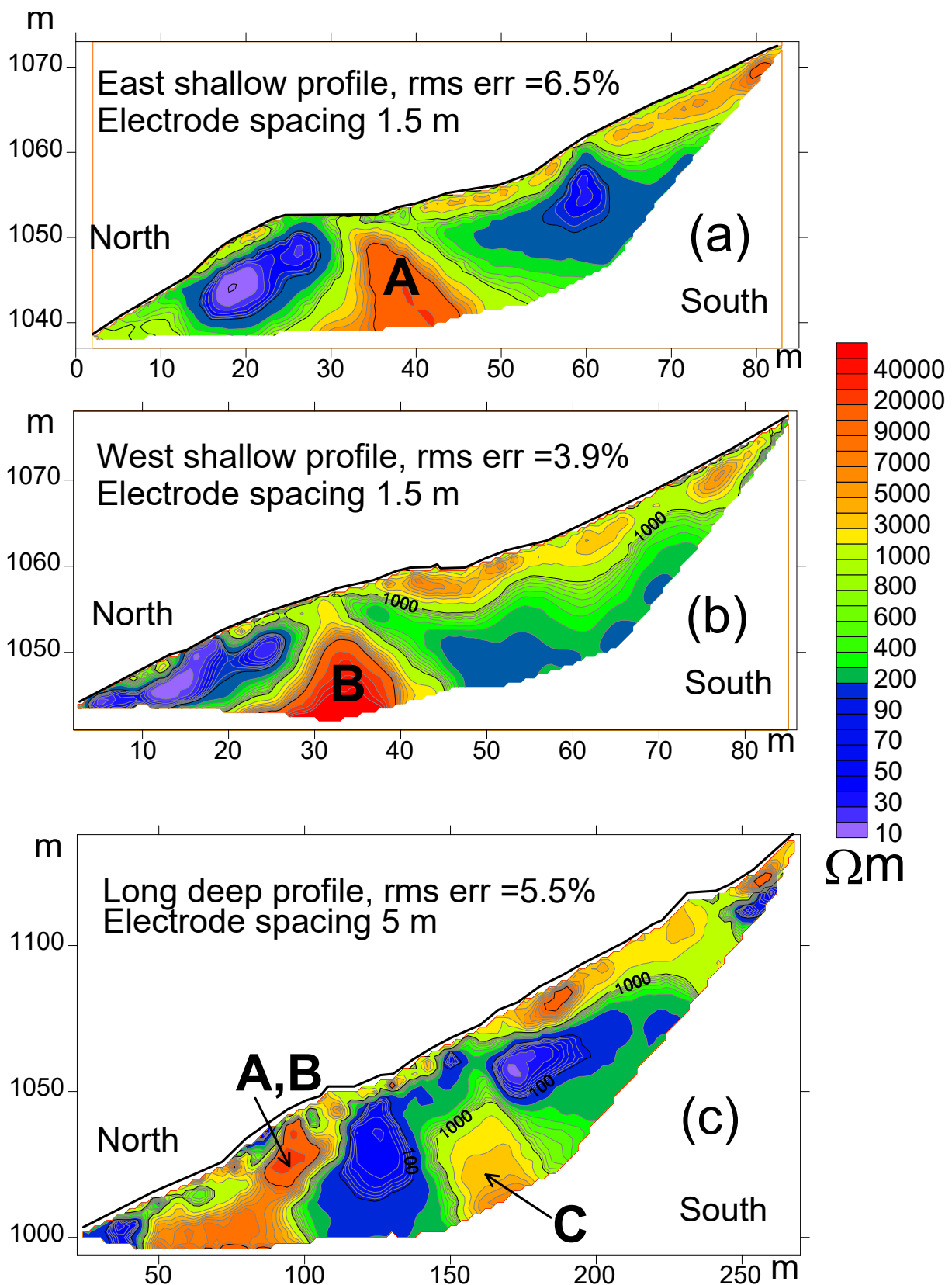
376 All data were acquired using a Terrameter GEOREVA LS23, which provides a
377 progressive pseudo-section display during acquisition (useful mainly for checking that
378 the measurement process is correct).

379 We first processed two parallel electrical resistivity tomographies (ERT) with 1.5 m
380 electrode spacing, Wenner-Schlumberger arrays with 64 electrodes, displayed along
381 the slope (descending from south to north). These two profiles are shown as black
382 lines in Fig. 4. The corresponding resistivity sections are shown in Fig. 9(a) and 9(b).

383 Later we processed a single long profile (also a Wenner-Schlumberger array) but
384 with 5 m electrode spacing along the more or less constant slope (Fig. 9 (c)). This
385 section is shown in Fig. 4 as a strictly N-S profile with black points used for real
386 electrode positions.

387 The results were obtained using RES2DINV (Loke 2000 and 2011).

388 In parts (a) and (b) a highly resistive body is shown in red (labelled A on the east
389 profile and B on the west profile). This body is likely to be less than 10m below the
390 surface. The same body is also clearly seen on the larger tomography (labelled A,B)
391 with a coherent shallow depth. The lower resistivities (in blue) are associated with
392 wet fractured rocks, while the higher resistivities at the surface are associated with
393 drained, drier colluvium, particularly on the upper part of the slope. In Fig. 9(c), the
394 larger and deeper tomography shows another body of high resistivity (resistivities
395 greater than 1000 Ω .m, labelled C) occurring at 20 - 30 m depth. This body is located
396 around the centre of the section.



397

398 **Fig. 9.** The two shallow ERTs are shown in (a) and (b) and reach a length of 94.5 m along
 399 the surface, while (c) shows the "deep section" with a length of 315 m. Anomalies A and B
 400 are most likely due to voids, as the interpreted resistivities can only be explained by such
 401 anomalies. In part (c), the deeper section again shows an anomaly associated with voids A
 402 and B. An additional resistivity body is now found in C, which could also be due to a cavity.

403 The interpreted resistivity is slightly lower than for the shallow suspected cavities, but this is
404 consistent with the size/depth ratio in this case. The deeper the body, the lower the resistivity
405 contrast.

406

407 It should be noted that this field survey was carried out over three years, with the two
408 shallow sections in the first year, the two gravimetric profiles in the second year with
409 this indication of a deeper cavity, and then in the third year we did the "deep" ERT
410 which shows this C anomaly indicating a deeper cavity if there is one.

411

412

413 **3. Results summary and discussion**

414

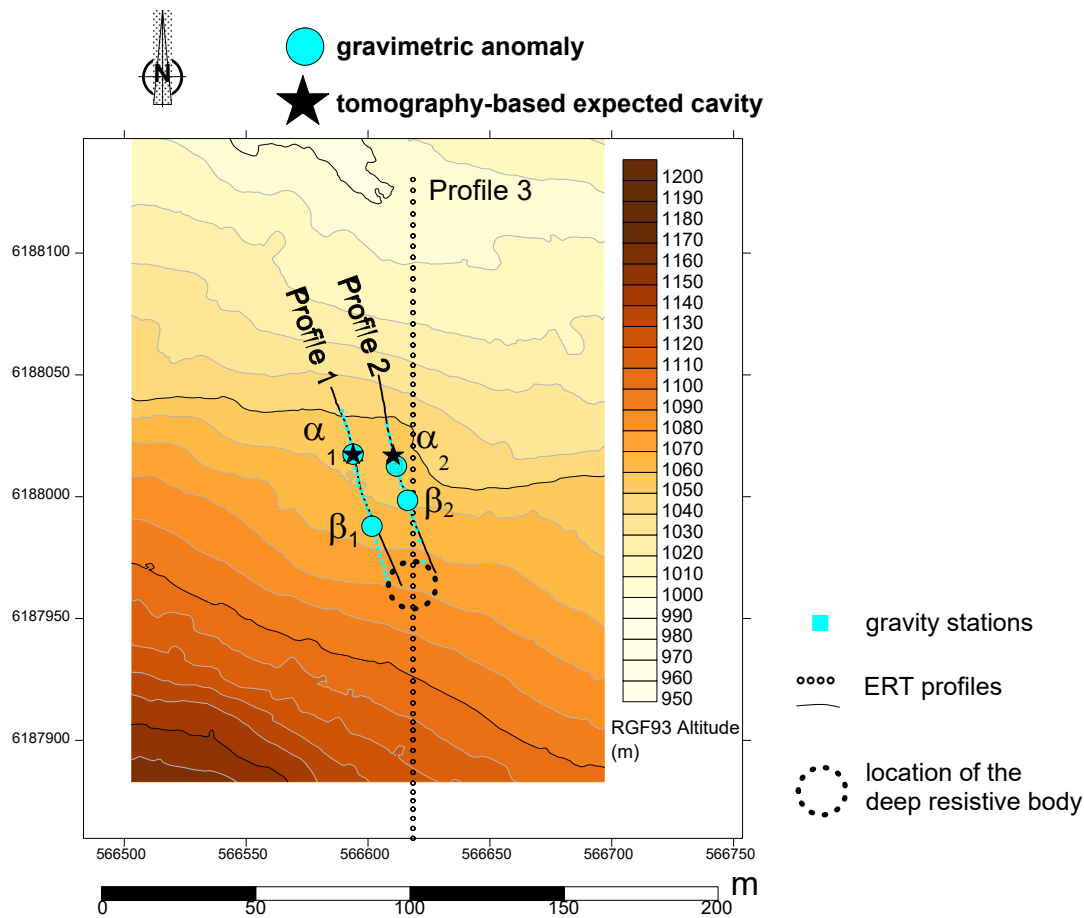
415 As far as inversion is concerned, we are (apparently) doing exactly the opposite of
416 what Tarantola (2006), from whom we quote, suggests: « Using observations to infer
417 the values of some parameters corresponds to solving an 'inverse problem'.

418 Practitioners usually seek the 'best solution' implied by the data, but observations
419 should only be used to falsify possible solutions, not to deduce any particular
420 solution. »

421 In fact, we fully agree with Albert Tarantola (who was our master in inversion) and we
422 believe that we have not found "the best solution". In a sense, we are doing the
423 opposite of what he suggests by "apparently deducing a particular solution"
424 (particularly for gravimetry). Definitely not. That is the point, we do not pretend to
425 deduce a solution, but only to offer a possible solution, just to provide an example of
426 a solution. We are fully aware of the limitations of geophysics, but we just want to
427 provide tools for dialogue with archaeologists and historians.

428 Only the α_1 and α_2 pair of cavities, probably revealed by gravimetry, appear to be
429 detected by the shorter electrical tomographies shown in Fig. 9(a) and 9(b).

430 Obviously, the second deeper pair of gravity anomalies, β_1 and β_2 , although clearly
431 visible on the gravity profiles, are not detected by these first two profiles of the
432 shallow ERT.



433

434

435 **Fig. 10.** Gravity station locations are shown as small blue squares, and the three ERT
 436 profiles are shown as small black dots. We have plotted the gravimetric anomalies as blue
 437 discs, and the tomographic expected cavity as a black star. We have a good match between
 438 the electrical and gravimetric anomalies α_1 and α_2 in the north, but no match for the
 439 gravimetric anomalies β_1 and β_2 . The black dotted circle indicates the location of the deep
 440 resistive body seen (anomaly C in Fig. 8(c)).

441

442 *It is clear that the northern anomalies, electrical and gravimetric, are superimposed*
 443 *within 2 or 3 metres (i.e. the resolution of the methods), and this is a real success of*
 444 *our investigation, which has made the existence of the cavity virtually certain.*

445 However, the two southern gravimetric anomalies, β_1 and β_2 , are isolated, without
 446 any correspondence with electrical anomalies.

447 It must be admitted that if there are caves here, they are not detected by the ERT. It
 448 is therefore difficult to say that the southern cavity is certain from a gravitational point
 449 of view. There could also be an electrical masking effect that prevents any electrical
 450 anomaly from being seen, and this is known to occur particularly when trying to
 451 detect resistive bodies at depth.

452 The aim of the third major ERT (Fig. 9(c)) was to electrically target this hypothetical
 453 deeper cavity seen by gravimetry. It is, so to speak, desired. However, this is not the

454 case, as shown in Fig. 10. On this profile we detect an unexpected deeper resistivity
455 anomaly, marked C on Fig. 9. It is too far away from the hypothetical void seen by
456 gravimetry to be interpreted as coming from a common source. Ultimately, an
457 additional gravimetric campaign would provide new insights, but this is not on the
458 agenda.

459

460 **4. Conclusion**

461

462 The aim of the geophysical survey was to confirm and locate old map indications of
463 currently covered pits and mine accesses. This objective has been achieved for at
464 least one pit, which is likely to be the northern pit (lower pit on the enlarged part of
465 ancient map, remembering that north is down on this historic map). In this case there
466 is excellent agreement between the high resistance electrical anomalies and the
467 gravimetric anomalies. This confirms the presence of cavities with almost certainty.
468 On the other hand, we cannot associate the triple consisting of: i) the southern
469 structure as seen on the old map; ii) the southern gravimetric anomalies; iii) the deep
470 resistive body, as there is no overlap between these three.

471 The use of geophysics in this archaeological survey has proved to be very efficient
472 and relevant in contributing to the knowledge of the old Ouels mine. This opens up
473 the possibility of a future mining archaeological operation, as the geophysical survey
474 has defined the area of interest, thus limiting the archaeological work, while
475 confirming the existence of a cavity that can be accessed by emptying the access
476 shaft. Despite the success of the geophysical survey, the archaeological operation
477 that was to confirm the data could not be undertaken for safety reasons. However,
478 the area is now defined as an archaeological reserve.

479

480

481 **Acknowledgements**

482
483 We would like to thank Jean-Charles Méaudre for the construction of the platform for
484 the installation of the gravimeter, without which this prospection would not have been
485 possible, and also Jurgen Heckes for the production of maps from several data sets
486 and for directing the photogrammetric and topographic campaign on the mining side
487 of Castel-Minier.

488
489 **References**

490
491 Bailly-Maître, M. C., Benoit, P., Les mines d'argent de la France médiévale. L'argent
492 au Moyen Age. Actes du XXVIII^e congrès de la Société des Historiens Médiévistes de
493 l'Enseignement Supérieur Public, Publications de la Sorbonne, Paris, 17-46.

494 Binley, A., Slater, L., 2020. Resistivity and Induced Polarization: Theory and
495 Applications to the Near-Surface Earth. Cambridge University Press, Cambridge.
496 <https://doi.org/10.1017/9781108685955>

497 Blakely, R.J., 1995. Potential Theory in Gravity and Magnetic Applications. Cambridge
498 University Press, Cambridge. <https://doi.org/10.1017/CBO9780511549816>

499 Bonnamour, G., Florsch, N., Téreygeol, F., 2007. Les prospections des ferriers de
500 Castel-Minier : approche interdisciplinaire. ArchéoSciences 37–44.
501 <https://doi.org/10.4000/archeosciences.712>

502 Dubatik, C., 1981. Recherches sur les travaux miniers du Haut Salat, 1re partie : Les
503 mines d'Aulus-Les-Bains, Autoédité. ed. Saliens.

504 Eppelbaum, L., 2010. Application of Microgravity at Archaeological Sites in Israel:
505 Some Estimation Derived from 3-D Modeling and Quantitative Analysis of Gravity
506 Field, Proceedings of the Symposium on the Application of Geophysics to Engineering
507 and Environmental Problems, SAGEEP. <https://doi.org/10.4133/1.3176721>

508 Flament, J., Mercier, F., Dubois, C., Téreygeol, F., 2019. Mining Archaeology and
509 Micro-Raman Analysis Associated with ESEM-EDX: Toward a Chrono-Spatial
510 Definition of Ore Consumption in a Pyrenean Medieval Workshop, 14th-16th
511 Centuries. Archaeometry 61, 99–116. <https://doi.org/10.1111/arcm.12404>

512 Florsch, N., Llubes, M., Téreygeol, F., 2012. Induced polarization 3D tomography of
513 an archaeological direct reduction slag heap. Surf. Geophys. 10.
514 <https://doi.org/10.3997/1873-0604.2012042>

515 Florsch, N., Llubes, M., Téreygeol, F., Ghorbani, A., Roblet, P., 2011. Quantification of
516 slag heap volumes and masses through the use of induced polarization: application to
517 the Castel-Minier site. J. Archaeol. Sci. 38, 438–451.
518 <https://doi.org/10.1016/j.jas.2010.09.027>

519 Higounet, C., 1947. Comté et Maison de Comminges entre France et Aragon au Moyen
520 Âge. Bulletin hispanique, 49, n° 3-4, 311-331. <https://doi.org/10.3406/hispa.1947.3102>

- 521 Hrubý, P., Kmošek, M., Kočárová, R., Košťál, M., 2021. Mediaeval mining centre of
522 Buchberg on Bohemian–Moravian Highlands. Metal production in The Kingdom of
523 Bohemia (13th-14th centuries), *Památky archeologické* 112:333-384.
524 DOI:10.35686/PA2021.
- 525 Laforet, C., Monchoux, P., Oudin, E., Tollon, F., 1983. Inventaire minéralogique de la
526 France n°11. Tome 1: bassin versant du Salat., BRGM. ed. Orléans.
- 527 Loke, M.H., 2011. Electrical resistivity surveys and data interpretation, Gupta, H. ed,
528 Solid Earth Geophysics Encyclopedia (2nd Edition) “Electrical & Electromagnetic.”
529 Springer-Verlag.
- 530 Loke, M.H., 2000. Electrical Imaging Surveys for Environmental and Engineering
531 Studies. A Practical Guide to 2-D and 3-D Surveys.
- 532 Nettleton, L.L., 1939. Determination of density for reduction of gravimeter
533 observations. *Geophysics*, 4, 3, 149-230, <https://doi.org/10.1190/1.0403176>.
- 534 Pašteka, R., Kušnirák, D., Wilken, D., Putiška, R., Papčo, J., Godová, D., Zvara, I.,
535 Nogová, E., Ondrášová, L., 2019. Effective combination of microgravimetry and
536 geoelectrical methods in the detection of subsurface cavities in archaeological
537 prospection – selected case-studies from Slovakia. *Contrib. Geophys. Geod.* 49, 479–
538 496. <https://doi.org/10.2478/congeo-2019-0025>
- 539 Pašteka, R., Pánisová, J., Zahorec, P., Papčo, J., Mrlina, J., Fraštia, M., Vargemezis,
540 G., Kušnirák, D., Zvara, I., 2020. Microgravity method in archaeological prospection:
541 methodical comments on selected case studies from crypt and tomb detection.
542 *Archaeol. Prospect.* 27, 415–431. <https://doi.org/10.1002/arp.1787>
- 543 Schlumberger, C. (1878-1936), 1920. Étude sur la prospection électrique du sous-sol.
544 Gauthier-Villars, Paris.
- 545 Tarantola, A., 2005. Inverse Problem Theory and Methods for Model Parameter
546 Estimation. Society for Industrial & Applied Mathematics, Philadelphia, PA.
- 547 Tarantola, A. 2006. Popper, Bayes and the inverse problem. *Nature Phys* 2, 492–494
548 (2006). <https://doi.org/10.1038/nphys375>
- 549 Téreygeol, F., 2023. “Bref ce sont les Indes Françaises...” (Malus, 1601) : Mines et
550 ateliers métallurgiques à Castel-Minier (X^e-XVI^e s.), Journées archéologiques
551 d’Ariège, Tarascon, 2023, p.122-142.
- 552 Trebsche, P., Schlögel, I., Flores-Orozco, A., 2022. Combining geophysical
553 prospection and core drilling: Reconstruction of a Late Bronze Age copper mine at
554 Priggwitz-Gasteil in the Eastern Alps (Austria). *Archaeological Prospection*, Volume
555 29, Issue 4 p. 557-577. <https://doi.org/10.1002/arp.1872>